Graph-Based Methods for Retinal Mosaicing and Vascular Characterization

Wendy Aguilar, M. Elena Martinez-Perez, Yann Frauel[1], Francisco Escolano, Miguel Angel Lozano[2], and Arturo Espinosa-Romero[3]

[1] Department of Computer Science, Insituto de Investigaciones en Matemáticas Aplicadas y en Sistemas, Universidad Nacional Autónoma de México, CP 04500
[2] Robot Vision Group. Universidad de Alicante, Spain
[3] Faculty of Mathematics, Universidad Autónoma de Yucatán. Anillo Periférico Norte. Tablaje Cat. 13615, Colonia Chuburná Hidalgo Inn. Mérida, Yucatán, México

Abstract. In this paper, we propose a highly robust point-matching method (*Graph Transformation Matching* - GTM) relying on finding the consensus graph emerging from putative matches. Such method is a two-phased one in the sense that after finding the consensus graph it tries to complete it as much as possible. We successfully apply GTM to image registration in the context of finding mosaics from retinal images. Feature points are obtained after properly segmenting such images. In addition, we also introduce a novel topological descriptor for quantifying disease by characterizing the arterial/venular trees. Such descriptor relies on diffusion kernels on graphs. Our experiments have showed only statistical significance for the case of arterial trees, which is consistent with previous findings.

1 Introduction

Image registration is a fundamental problem to several image processing and computer vision applications. In the case of medical retinal images, two images taken before and after laser surgery can be registered to detect location of lesions. Two images taken from the same eye but at different times can be registered to quantify the severity of disease and the progression of therapy. A series of images of the same retina can be registered to form a mosaic image giving a complete view of the retina. The quantification of some diseases is commonly made by measuring differences in tree vascular structure between groups. Measurements can be either geometrical or topological [9].

In this paper we present a twofold graph-based method applied to retinal image analysis: 1) a graph-based point-matching algorithm to allow the construction of mosaics in order to have a larger view of the retina, and 2) a tree vascular characterization in order to find structural differences such as those found by other authors [4,5]. The graph-based point-matching algorithm, *Graph Transformation Matching* (GTM), is an efficient method for dealing with high rates of outlying matches, which is the main drawback of some continuation methods for graph matching like *Softassign*, or its kernelized version [7], which

F. Escolano and M. Vento (Eds.): GbRPR 2007, LNCS 4538, pp. 25–36, 2007.

optimize quadratic cost functions. In addition to the latter, we propose a new spectral descriptor relying on diffusion kernels for characterizing the topologies of normotensive and hypertensive arterial trees.

The rest of the paper is organized as follows. Section 2 describes the process of segmenting vascular trees (arterial and venular) and extracting the key features from retinal images, which is a critical step for further analysis. Section 3 describes the *Graph Transformation Matching*: (i) the basic approach, (ii) the optimized algorithm, and (iii) the recovery phase. We test the algorithm in the context of retinal image alignment and compare it with *Softassign*. Section 4 is devoted to describe the interpolation method used for the alignment to generate a mosaic view. Section 5 presents our spectral descriptor for vascular characterization and show its adequacy. Finally, in Section 6 we outline our conclusions.

2 Image Feature Extraction

Previous work has been done in order to analyze and extract features from retinal images. The process consists of two main steps: i) the segmentation of blood vessels to generate a binary image, and ii) the analysis of the binary image. Features of interest herein are branching and crossing points as feature points for mosaicing and, extraction of arterial and venous vessel trees for characterization. Blood vessels are segmented based on a multi-scale analysis of the first and second derivatives of the images in combination with a region growing algorithm [10]. Figs. 1(a) and 1(c) show two different views of retinal images and Figs. 1(b) and 1(d) their segmented binary images, respectively. The optic disc region is on the bottom-left, vessels are tracked from this area outwards.

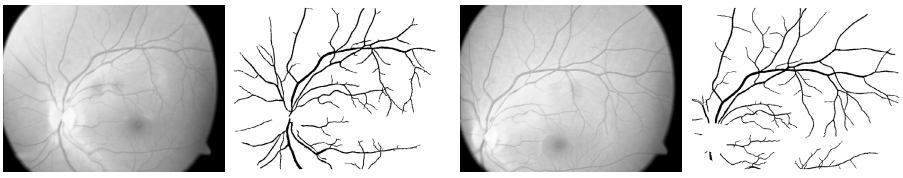

(a) (b) (c) (d)

Fig. 1. Retinal images. (a) *img15* and (c) *img21* are two different views from the same eye-ball and, (b) and (d) are their respective segmented binary images.

A semi-automatic method to measure and quantify geometrical and topological properties of continuous vascular trees on binary retinal images was developed on a previous work [9]. The analysis of the binary image involves: i) labelling each vessel tree, ii) detecting significant points, iii) extracting the vessel tree by a chain code tracking method and iv) measuring geometrical and topological parameters.

Labelling each vessel tree involves thinning the segmented binary image to produce its skeleton. Three types of significant points in the skeleton must be

detected: terminal, bifurcation and crossing points. In a first pass, skeleton pixels with only one neighbor in a 3×3 neighborhood are labelled as terminal points and pixels with 3 neighbors are labelled as candidate bifurcation points. Fig. 2(a) shows the skeleton of the tree with the candidate points marked with circles.

Because vessel crossing points appear in the skeleton as two bifurcation points very close to each other, a second pass is made using a fixed size window centered on the candidate bifurcations. The number of intersections of the skeleton with the window frame determine whether the point is a bifurcation or a crossing. After this process a chain code is used to label the rest of the skeleton points in order to track the tree. Fig. 2(b) shows the branching and crossing points marked with circles over the skeleton and the tree tracked on black. Finally, after the tracking process the selected tree is isolated. Fig. 2(c) shows an arterial tree extracted. The user should select the tree to be tracked and decided if it is an arterial or a venous tree.

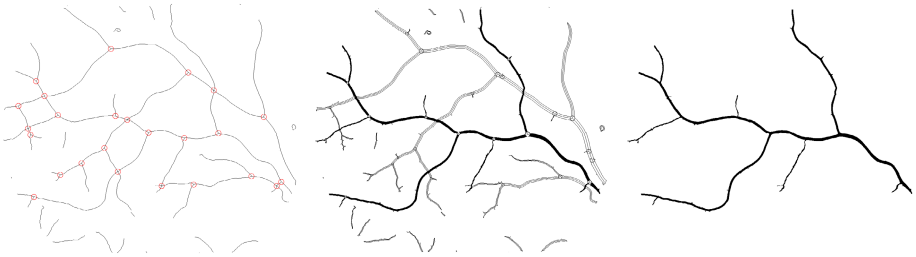

(a) (b) (c)

Fig. 2. Binary image analysis: (a) skeleton with candidate points marked with circles, (b) branching and crossing points marked with circles and tracked tree marked in black. (c) arterial tree extracted.

3 Graph Transformation Matching

Once significant points have been detected in both images, we proceed to get an initial matching between them. This can be done by making a cross-correlation around each significant point and matching with the point having the highest correlation value. From this process two sets of corresponding points $P = \{p_i\}$ and $P' = \{p'_i\}$ of size N (where p_i matches p'_i) are found. The *Graph Transformation Matching* (GTM) algorithm consists of two phases: a pruning and a recovering phase. In the pruning phase, a *median K-NN graph* $G_P = (V_P, E_P)$ is computed as follows: vertices $V_P = v_1, ..., v_N$ are given by the positions of the N corresponding points. A non-directed edge (i, j) exists when p_j is one of the K closest neighbors of p_i and also $||p_i - p_j|| \leq \eta$. Being $\eta = med_{(l,m)\in V_P \times V_P} ||p_l - p_m||$ the median of all distances between pairs of vertices. The first condition states that a vertex can just validate the structure of its closest neighbors, while the second condition restricts the proximity of validation which filters structural deformations due to outlying points. If there are not K vertices that support the

structure of p_i then this vertex is disconnected completely. The graph G_P, which is not necessarily connected, has the $N \times N$ adjacency matrix A_{ij}, where $A_{ij} = 1$ when $(i, j) \in E_P$ and $A_{ij} = 0$ otherwise. Similarly, the graph $G_{P'} = (V_{P'}, E_{P'})$ for points p'_i has adjacency matrix A'_{ij}, also of dimension $N \times N$ because of the one-to-one initial matching M.

GTM relies on the hypothesis that outlying matchings in M may be removed, with high probability, by iteratively applying a simple structural criterion [1]. Thus, GTM iterates as follows: (i) selecting an outlying matching; (ii) removing matched features corresponding to the outlying matching, as well as this matching itself, and (iii) recomputing both *median K-NN graphs*. Structural disparity is approximated by computing the residual adjacency matrix $R_{ij} = |A_{ij} - A'_{ij}|$ and selecting column $j^o = argmax_{j=1...N} \sum_{i=1}^{N} R_{ij}$, the one that yields the maximal number of different edges in both graphs. The selected structural outliers are the features forming the pair (p_{j^o}, p'_{j^o}). Thus, we remove v_{j^o} from G_P and v'_{j^o} from $G_{P'}$, and (p_{j^o}, p'_{j^o}) from M. Then, after decrementing N, a new iteration begins, and the median *K-NN graphs* are computed from the surviving vertices. The algorithm stops when it reaches the null residual matrix, that is, when $R_{ij} = 0, \forall i, j$. It seeks for finding a *consensus graph* and returns the number of vertices of this graph. Fig. 3 shows an example of the transformation process for two retinal images, from iteration 0 (initial graphs) to iteration 71 (final identical graphs), with $K = 4$ which showed to be adequate in all our experiments.

An example of initial and final matchings for two pairs of retinal images are shown in Figs. 4 (a) and (b) for images named *img15* and *img12*, and Figs. 4 (c) and (d) for *img15* and *img21*. Fig. 5 shows their respective resulting graphs.

Considering that the bottleneck of the algorithm is the re-computation of the graphs, which takes $O(N^2 logN)$ (the same as computing the median at the beginning of the algorithm) and also that the maximum number of iterations

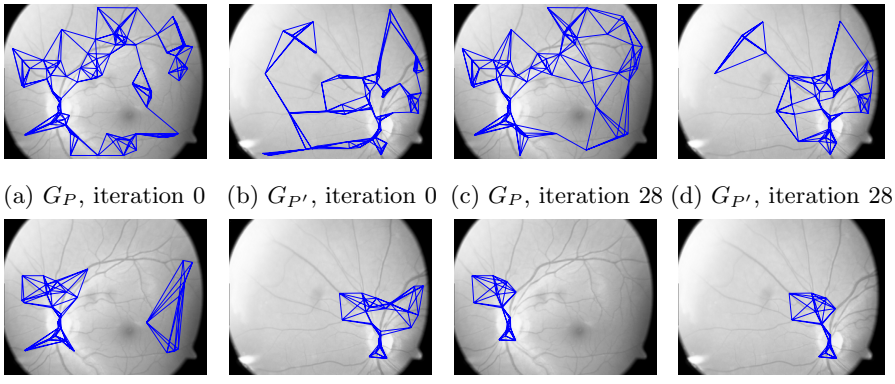

(a) G_P, iteration 0 (b) $G_{P'}$, iteration 0 (c) G_P, iteration 28 (d) $G_{P'}$, iteration 28

(e) G_P, iteration 56 (f) $G_{P'}$, iteration 56 (g) G_P, iteration 71 (h) $G_{P'}$, iteration 71

Fig. 3. Graph Transformation process example. G_P corresponds to the *median K-NN graph* of *img15* and $G_{P'}$ for *img12* during iterations 0, 28, 56 and 71.

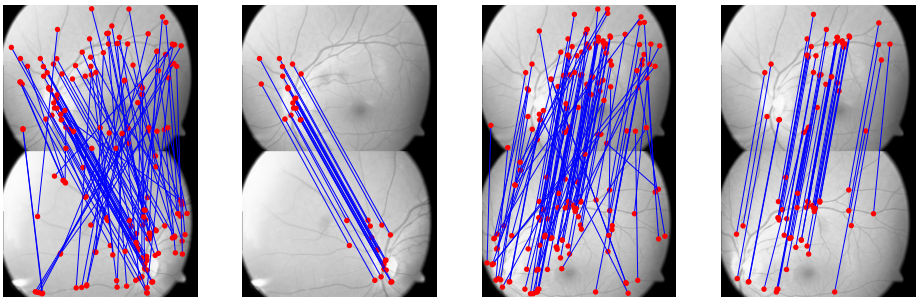

(a) Initial matches, *img15* with *img12* (b)Final matches, *img15* with *img12* (c) Initial matches, *img15* with *img21* (d) Final matches, *img15* with *img21*

Fig. 4. GTM initial and final matches from the pruning phase: (a)-(b) *img15* with *img12* and (c)-(d) *img15* with *img21*

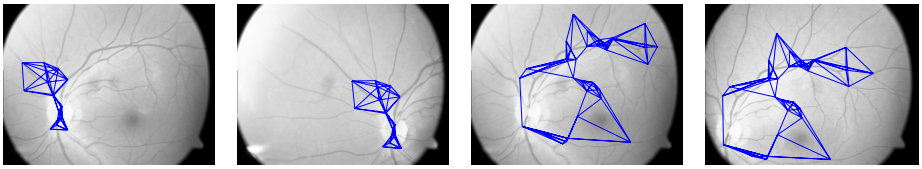

(a) G_P for matching *img15* with *img12* (b) $G_{P'}$ for matching *img15* with *img12* (c) G_P for matching *img15* with *img21* (d) $G_{P'}$ for matching *img15* with *img21*

Fig. 5. Graphs resulting from GTM in its pruning phase: (a)-(b) *image15* with *image12* and (c)-(d) *image15* with *image21*

is N, the worst case complexity is $O(N^3 logN)$. A significant improvement in the reconstruction of the graphs was made. It consists of replacing the graph representation (adjacency matrix) by three new structures: i) a matrix O_F of size $n \times n$ where rows represent output edges for each vertex (ordered by distances smaller than the median and where the first K locations represent the actual output edges for that vertex, the rest are the potential next connections), ii) an array of linked lists I_F of dimension n with input edges for each vertex and iii) an array N_F of dimension n that keeps a reference to the next available edge to connect in O_F (initially with value $K + 1$).

Two implementations were made (in C language), one corresponding to the brute force algorithm and the other to the optimized version. The time required for the algorithm depends on two variables: i) the number of initial vertices (which is directly related to the number of matches) and ii) the number of iterations. To test the significance of the optimization, two experiments were made by fixing one factor at a time. Time results for both implementations (in seconds) are shown in Fig. 6, (a) and (b). These graphs make evident the improvement in time due to the optimization of the algorithm. The difference was

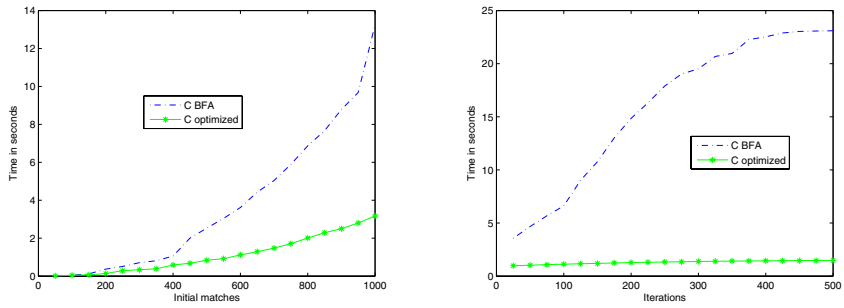

(a) Number of iterations fixed to 40 (b) Initial matches fixed to 559

Fig. 6. Graphs of times reported for GTM algorithms implemented in *C*: (a) brute force and (b) optimized

more significant in the second case (b) suggesting an almost constant behavior of the optimized version versus the increasing time of the brute force version.

In addition to the efficiency desired for the proposed matching algorithm, it was also wanted to make it robust to a large amount of outliers. To test the latter, an experiment was made consisting of taking a set of 60 correct matches and introduce different percentages of outliers randomly generated, from 10% to 95%. Results showed that in the case of 85% of outliers, the *Graph Transformation* algorithm could recover 48 correct matches (from the 60 available) with just 2 mismatches. In the case of 95% of outliers it recovered 24 with 2 mismatches. Images used in this paper contain at most 74% of natural outliers. For some applications it is wanted to recover high quantities of correct matches

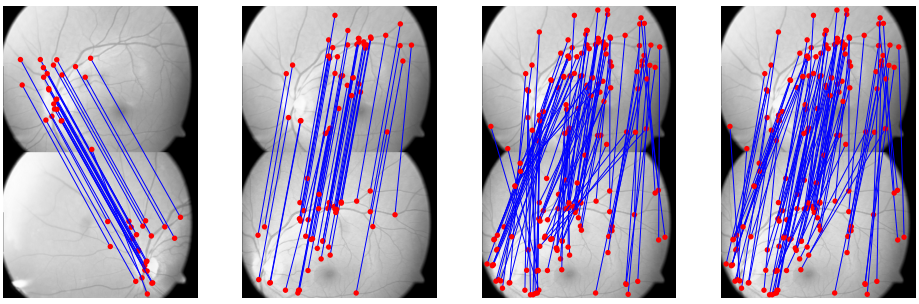

(a) After recovery, *img15* with *img12* (b) After recovery, *img15* with *img21* (c) Just structure, *img15* with *img12* (d) Using kernels, *img15* with *img12*

Fig. 7. (a)-(b) Results from the recovery phase when matching (a) *img15* with *img12* and (b) *img15* with *img21*. (c)-(d) *Softassign* results from matching *img15* with *img12 using (c) just structure and (d) kernels.*

tolerating some mismatches. For these cases, here we propose a second phase of the GTM algorithm named *Recovering Phase*. It consists in taking final graphs and matches obtained from the pruning phase and adding iteratively all rejected matches one at a time, recomputing the corresponding *K-NN graphs* and testing the residual matrix condition. If this condition is satisfied, then this match is considered as correct. Otherwise, it is discarded. Figs. 7 (a) and (b) show the resulting matchings after the recovery phase for *img15* with *img12* and *img15* with *img21*. Compare these results with those showed in Figs. 4 (b) and (d).

We compared our results versus those obtained from the *Softassign* algorithm. Figs. 7(a) and (b) present the results obtained from matching *img15* with *img12*, using *Softassign* with (a) just structure and (b) kernels. In the case of using kernels and costs, the resulting matching was exactly the same as the input, suggesting that the costs completely influence the matching process. Figs. 7(c) and (d) show the contribution of the recovery phase.

The algorithm was also tested with other retinal images. Some of the results are shown in Figs. 8 and 9.

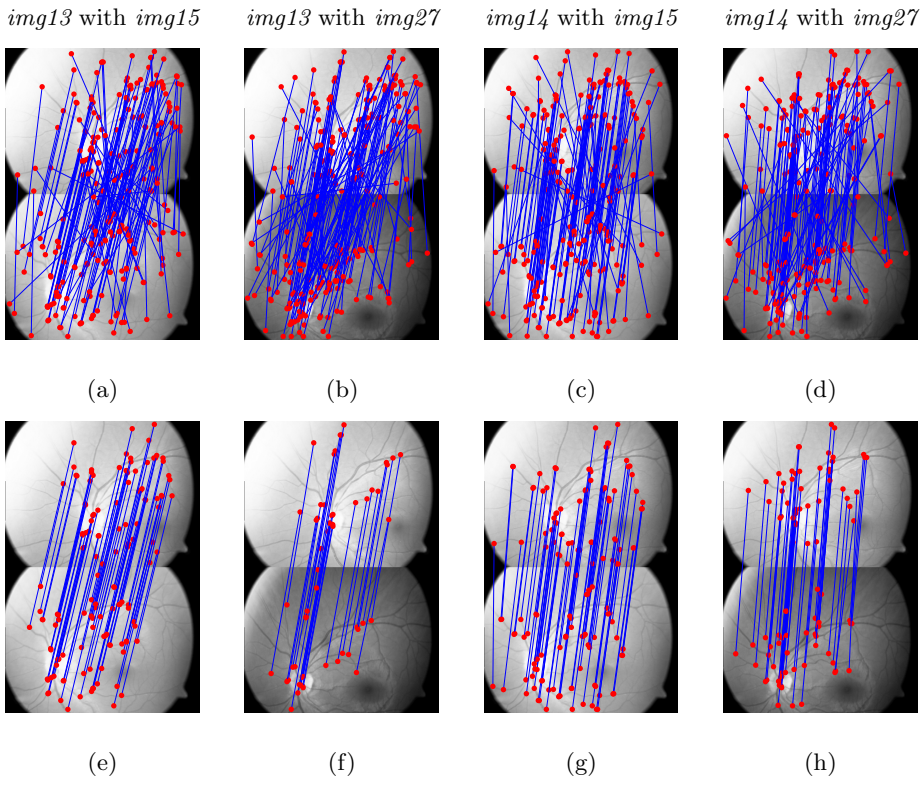

Fig. 8. Other matching results. (a)-(d) show the initial matches and (e)-(h) show the corresponding final matches from *GTM* algorithm.

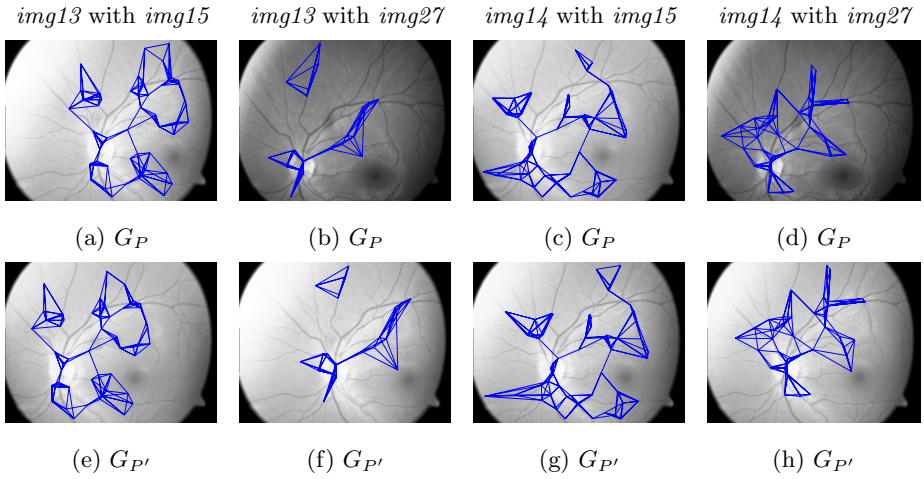

(a) G_P (b) G_P (c) G_P (d) G_P

(e) $G_{P'}$ (f) $G_{P'}$ (g) $G_{P'}$ (h) $G_{P'}$

Fig. 9. Resulting graphs from *GTM* algorithm of other results

4 Mosaicing

The retinal images used in this section were taken using a fundus camera with a 50° field of view (Zeiss FF 450 IR). Images were acquired with a CCD camera (Sony Power HAD 3CCD Color Video Camera) attached to the fundus camera with 768×576 pixels in size. Since the surface of the retina is curved, almost spherical, the interimage transformation model use to build the mosaic must take this into account.

A quadratic model surface is a good approximation that allows corrections of misalignment of blood vessels that cannot be corrected on spherical surface by rotation, translation and scale modifications only. Based on the matched points computed from the GTM technique, a pair of functions that maps a pixel position (x, y) to a new position (x', y') is found. We will use the three images showed in Fig. 4 (*img15*, *img12* and *img21*) to build the mosaic using *img15* as the reference coordinate system.

A quadratic transformation is applied between the reference image and the images to be changed into its coordinate system. The functions are defined as the polynomial equations:

$$\begin{aligned} x' &= \sum_{i=0}^{m} \sum_{j=0}^{m-i} a_{ij} x^i y^j, \\ y' &= \sum_{i=0}^{m} \sum_{j=0}^{m-i} b_{ij} x^i y^j, \quad m = 2 \end{aligned} \tag{1}$$

where (x, y) and (x', y') are set of corresponding points in the original image and the corrected image, respectively. A number of N coordinates are collected from both images and, by substituting them in equations 1, a set of N linear equations with respect to the coefficients $a_{i,j}$ and $b_{i,j}$ are obtained. The solution is found by least squares criterion and an approximation of the functions that

describe the correct mapping is found. The mapping is expressed in terms of a pair of transformation maps, (M_x, M_y), that record the correspondence between every pixel in the original image $I(x, y)$ and the corrected image $I'(x, y)$:

$$I'(x, y) = I(M_x(x, y), M_y(x, y)) \tag{2}$$

The final image obtained from mosaicing *img12*, *img15* and *img21* is shown in Fig. 10.

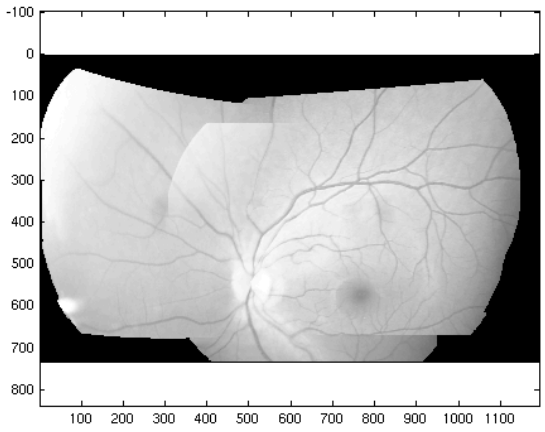

Fig. 10. The result mosaic after matching images *img15* with *img12* and with *img21*

5 Spectral Vascular Characterization

Previous approaches [4,9] to quantify changes in vascular trees due to disease are mainly focused on geometric parameters (branching angles, length-to-diameter ratio, diameter, and so on) whereas topological measurements (e.g. asymmetry, number of terminal branches) have been less studied [5,9]. We propose a new topological measure based on the computation of diffusion kernels [2,6] on binary trees. Images used in this section were obtained from [8]. 20 images (10 normotensive and 10 hypertensive) were taken using a fundus camera with 30° field of view (Kowa FX-50R). Photographic negatives were digitized and reduced to 533×509 pixels size. Vessel trees were segmented and extracted as described in section 2.

Given a tree $T = (V, G)$ with: m vertices, adjacency matrix A and Laplacian L where: $L_{ij} = -1$ when $(i, j) \in E$, $L_{ii} = \sum_i A_{ij}$, and $L_{ij} = 0$ otherwise, the diffusion kernel K of A is defined by the matrix exponentiation of the Laplacian:

$$K \equiv e^{-\beta L} = I_m + L + \frac{1}{2!}L^2 + \frac{1}{3!}L^3 + \ldots, \tag{3}$$

being I_m the $m \times m$ identity matrix. In the particular case of an infinite binary tree, we have that the kernel value between two vertices i and j depends on the length d_{ij} of the unique path connecting them [3,6]:

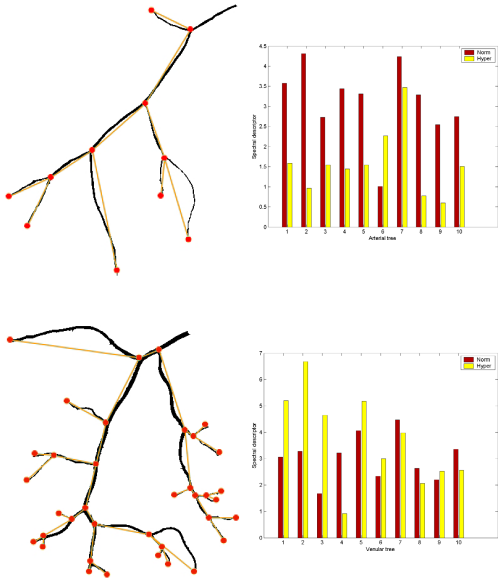

Fig. 11. Characterization. Left: Examples of hypertense (up) and normotensive (down) arterial trees. Right: Spectral Descriptor for arterial (up) and venular (down) trees.

$$K_{ij} = K^2(d_{ij}) = \frac{2}{\pi}\int_0^\pi \frac{e^{-\beta(1-\cos x)}}{4(1-\cos^2 x)} \sin x[\sin(d_{ij}+1)x - \sin(d_{ij}-1)x]dx$$
$$K_{ii} = K^2(0) = \frac{1}{\pi}\int_0^\pi e^{-\beta(1-\cos x)}dx \tag{4}$$

Equation 4 shows a well known property of kernels on trees. Alike in terms of random walks, K_{ij} can be regarded as the probability that a *lazy* random walk reaches j from i, in binary trees, where there is a unique path between two nodes. Such probability depends on the length of the path, because the branching factor is constant. In the infinite case, K_{ii} is constant but this does not happen in the finite case where K_{ii} is given by $1 - \sum_j K_{ij}$ and the distribution of distances d_{ij} is not uniform. In addition, for the $i-$th node in the tree, the coefficients $\{K_{ij}, j = 1 \ldots m\}$ define a spectral signature, in this case a probability density function specifying the probability of reaching each node in the tree from the $i-$th one. For the application domain considered in this paper, we propose to quantify the comparison of the $\{K_{ij}\}$ probability distribution functions of vertices from normotensive and hypertensive trees with those associated to nodes in perfect binary trees with the same cardinality, say m. Such comparison will yield path-length invariance when characterizing a given binary tree, but it requires to properly mapping each tree on the perfect one (completely balanced), a sort of simple tree matching. After such matching, if the $i-$th node in the tree is mapped on i' in the perfect tree, a simple *spectral tree descriptor* is given by:

$$SD(T) = \sum_{i=1}^{m} (H_i^{K_T} - H_{i'}^{K_P})^2 \text{ being } H_i^K = \sum_{j=1}^{m} K_{ij} \log K_{ij}. \quad (5)$$

where: K_T is the diffusion kernel of the tree and K_P is the one of the perfect binary tree with the same number of nodes; H^{K_T} and H^{K_P} are the entropies of the probability distributions associated to the vertices and induced by the kernels [7]. In Fig. 11 we show our preliminary characterization experiments. We have considered both arterial and venular trees for 10 normotensive and 10 hypertensive subjects. After the Wilcoxon rank test, only statistically significant differences ($p < 0.0211$) where found in arterial trees. However, when comparing descriptors corresponding to venular trees the differences where no significant ($p = 0.3847$). These findings are consistent with the evidence already reported of geometrical and topological parameters [8], and show that the new spectral descriptor may complement existing measures.

6 Conclusions

We have presented both a novel graph-based algorithm applied to the match of correspondence points for retinal mosaicing, and a structural characterization of retinal tree vasculature. On one hand, the results obtained for mosaicing depend on the amount of overlapping regions between images and on the number of matching points. Further work has to be done in order to obtained larger views and more robust results using more matching points to get better mapping approximations. The GTM algorithm has demonstrated to be a fast, robust and reliable method for feature matching. On the other hand, the analysis of purely topological indices of retinal blood vessels made by [8,9], using the same database, showed that arterial and venous trees are asymmetric and indices such as the number of terminal edges not including the root: N_T, the total sum of external path length in the tree: P_e, and the total number of external-internal edges: E_I, can characterize normal arterial trees from those of hypertensive subjects. They displayed no differences in topology for venous trees between groups. However, it is known that the latter topological indices are tree size dependent and thus a normalization factor should be applied. On the contrary, the spectral descriptor presented in this paper, which is consistent with previous findings, is size invariant and it has proved to be effective. Such descriptor can be considered another useful measurement as a complement for the analysis of geometry.

Acknowledgments

Authors would like to thank to *Clinica Lomas Altas* at México, D.F. who provided us with the images used for mosaicing and to *Department of Clinical & Cardiovascular Pharmacology* at St. Mary's Hospital, London for the clinical images use in the vascular characterization.

References

1. Aguilar, W.: Object recognition based on the structural correspondence of local features. Master's thesis, UNAM, Mexico city (2006)
2. Chung, F.R.K.: Spectral graph theory. In: Conference Board of Mathematical Science CBMS, Providence, RI, American Matematical Society, vol. 92 (1997)
3. Chung, F.R.K., Yau, S.-T.: Coverings, heat kernels and spanning trees. Electronic Journal of Combinatorics, 6 (1999)
4. Gelman, R., Martinez-Perez, M.E., Vanderveen, D.K., Moskowitz, A., Fulton, A.: Diagnosis of plus disease in retinopathy of prematurity using retinal image multisacle analysis (risa). Investigative Ophthalmology & Visual Science 46(12), 4734–4738 (2005)
5. Hughes, A.D., Martinez-Perez, M.E., Jabba, A.-S., Hassan, A., Witt, N.W., Mistry, P.D., Chapman, N., Stanton, A.V., Beevers, G., Pedrinelli, T., Parker, K.H., Thom, S.A.M.: Quantification of topological changes in retinal vascular architecture in essential and malignant hypertension. Journal of Hypertension 24(5), 889–894 (2006)
6. Kondor, R., Lafferty, J.: Diffusion kernels on graphs and other discrete input spaces. In: Proc. Intl. Conf. on Machine Learning, Los Altos CA, pp. 315–322 (2002)
7. Lozano, M.A., Escolano, F.: A significant improvement of softassign with diffusion kernels. In: Fred, A., Caelli, T.M., Duin, R.P.W., Campilho, A., de Ridder, D. (eds.) Structural, Syntactic, and Statistical Pattern Recognition. LNCS, vol. 3138, pp. 76–84. Springer, Heidelberg (2004)
8. Martinez-Perez, M.E.: Computer Analysis of the Geometry of the Retinal Vasculature. PhD thesis, Imperial College, London, UK (2001)
9. Martinez-Perez, M.E., Hughes, A.D., Stanton, A.V., Thom, S.A., Chapman, N., Bharath, A.A., Parker, K.H.: Retinal vascular tree morphology: A semi-automatic quantification. IEEE Transactions on Biomedical Engineering 49(8), 912–917 (2002)
10. Martinez-Perez, M.E., Hughes, A.D., Thom, S.A., Bharath, A.A., Parker, K.H.: Segmentation of blood vessels from red-free and fluorescein retinal images. Medical Image Analysis 11(1), 47–61 (2007)